Temporal regulation of morphogenetic events in *Saccharomyces cerevisiae*

Helen Lai[a,b], Jian-Geng Chiou[a], Anastasia Zhurikhina[c], Trevin R. Zyla[a], Denis Tsygankov[c,*], and Daniel J. Lew[a,b,*]

[a]Department of Pharmacology and Cancer Biology and [b]Department of Molecular Genetics and Microbiology, Duke University, Durham, NC 27710; [c]Wallace H. Coulter Department of Biomedical Engineering, Georgia Institute of Technology and Emory University School of Medicine, Atlanta, GA 30332

ABSTRACT **Tip growth in fungi involves highly polarized secretion and modification of the cell wall at the growing tip. The genetic requirements for initiating polarized growth are perhaps best understood for the model budding yeast *Saccharomyces cerevisiae*. Once the cell is committed to enter the cell cycle by activation of G1 cyclin/cyclin-dependent kinase (CDK) complexes, the polarity regulator Cdc42 becomes concentrated at the presumptive bud site, actin cables are oriented toward that site, and septin filaments assemble into a ring around the polarity site. Several minutes later, the bud emerges. Here, we investigated the mechanisms that regulate the timing of these events at the single-cell level. Septin recruitment was delayed relative to polarity establishment, and our findings suggest that a CDK-dependent septin "priming" facilitates septin recruitment by Cdc42. Bud emergence was delayed relative to the initiation of polarized secretion, and our findings suggest that the delay reflects the time needed to weaken the cell wall sufficiently for the cell to bud. Rho1 activation by Rom2 occurred at around the time of bud emergence, perhaps in response to local cell-wall weakening. This report reveals regulatory mechanisms underlying the morphogenetic events in the budding yeast.**

Monitoring Editor
Rong Li
Johns Hopkins University

Received: Mar 26, 2018
Revised: Jun 4, 2018
Accepted: Jun 11, 2018

INTRODUCTION

Many of the signature achievements of cells and organisms rely on the execution of precisely ordered series of events. For example, metabolic pathways synthesize complex molecules through ordered series of reactions in which the product of one reaction creates the substrate for the next reaction (Berg *et al.*, 2015). In these and other instances, each step is dependent upon completion of a prior step. In a different example, successful cell multiplication involves the ordered duplication and segregation of chromosomes prior to cell division during the cell cycle (Morgan, 2007). In that case, the ordering of events arises from regulated increases and decreases in the activity of master regulatory cyclin-dependent kinases (CDKs), constituting an independent timer that triggers different events in their proper order. Here we address the mechanisms dictating the timing of the events that contribute to bud emergence, an essential morphogenetic step during the cell cycle in the budding yeast *Saccharomyces cerevisiae*.

Bud emergence involves several events that appear to occur in a reproducible order (Pringle *et al.*, 1995; Chen *et al.*, 2012). First, cells establish a polarity site marked by the local accumulation of polarity factors including the master regulatory GTPase Cdc42 (Chiou *et al.*, 2017). The formin Bni1, an actin nucleator, then localizes to the polarity site and generates actin cables (linear bundles of parallel actin filaments) oriented toward that site (Pruyne *et al.*, 2004b). The actin cables act as tracks for the delivery of secretory vesicles, which accumulate near the polarity site (Pruyne *et al.*, 2004b). Septin proteins, which also assemble into filaments, accumulate and form a ring surrounding Cdc42 at the polarity site to recruit multiple proteins to the mother-bud neck and to support the structure of the bud (Oh and Bi, 2011; Howell and Lew, 2012). Bud

This article was published online ahead of print in MBoC in Press (http://www.molbiolcell.org/cgi/doi/10.1091/mbc.E18-03-0188) on June 21, 2018.

*Address correspondence to: Daniel J. Lew (daniel.lew@duke.edu) or Denis Tsygankov (denis.tsygankov@bme.gatech.edu).

Abbreviations used: CDK, cyclin-dependent kinase; Con A, concanavalin A; CWI, cell wall integrity pathway; DIC, differential interference contrast; 5FOA, 5-fluoroorotic acid; GEF, guanine nucleotide exchange factor; GFP, green fluorescent protein; GTP, guanosine triphosphate; GUI, graphic user interface; ROI, region of interest; TOI, time of interest.

emergence itself occurs several minutes later and involves modifications of the cell wall overlying the polarity site (Smits *et al.*, 1999).

Studies using mutants and drugs that perturb polarity or cytoskeletal factors have shown that whereas both the actin and the septin reorganizations that precede bud emergence are dependent upon Cdc42 (Adams *et al.*, 1990; Iwase *et al.*, 2006), actin polarization can occur in the absence of septins (Adams and Pringle, 1984), and septin ring formation can occur in the absence of F-actin (Ayscough *et al.*, 1997), so these events are not obligatorily linked. Nevertheless, there is evidence that actin-mediated vesicle delivery contributes to proper septin ring assembly (Kadota *et al.*, 2004; Kozubowski *et al.*, 2005; Iwase *et al.*, 2006; Gao *et al.*, 2007; Okada *et al.*, 2013) and that septins contribute to the assembly of oriented actin cables (Pruyne *et al.*, 2004a; Chesarone and Goode, 2009). It is unclear whether these cytoskeletal cross-talk pathways act during normal assembly of the polarized cytoskeleton or whether they are needed to maintain the structures once they have formed.

Bud emergence requires the local modification of the cell wall. Once polarized, actin and septins lead to modifications of the yeast cell wall, an elastic structure that confers cell shape and provides a selective barrier to the passage of large molecules (Lesage and Bussey, 2006). Yeast cells are under turgor caused by the influx of water in response to an osmotic gradient between the cell and its environment (Harold, 1990, 2002). The turgor pushes the plasma membrane out against the cell wall, expanding it until the glucan cage resists the pressure. A bud forms when the local cell wall overlying the polarity site is weakened by secreted hydrolases, allowing the pressure to generate a bulge. Actin-mediated delivery of secretory vesicles promotes local cell-wall remodeling (Lesage and Bussey, 2006), and septin-mediated localization of chitin synthase III promotes formation of the chitin ring (also called bud scar) at the base of the emerging bud (DeMarini *et al.*, 1997). Thus, polarity establishment leads to cytoskeletal remodeling that promotes localized cell-wall changes leading to bud emergence.

Single-cell imaging suggests that there is considerable cell-to-cell variability in the timing of polarization of cytoskeletal elements (Chen *et al.*, 2012), so it is not clear whether there is a reproducible order of polarization events or whether some cells may exhibit alternative orders of events. To gain insight into whether bud emergence requires a precisely ordered series of events, and to understand why and how some events might occur at different times relative to others, we examined the events leading to bud emergence at high temporal resolution. Our findings suggest that these morphogenetic events are indeed ordered, and some events are regulated by an independent timer, whereas the initiation of other events depends on the completion of previous events.

RESULTS

Measuring the timing and dynamics of morphogenetic events

To examine the timing of morphogenetic events, we imaged strains bearing fluorescent probes for polarity establishment (the polarity scaffold protein Bem1; Kozubowski *et al.*, 2008), actin-dependent secretory vesicle polarization (the Rab GTPase Sec4; Chen *et al.*, 2012), and septin organization (the septin Cdc3; Caviston *et al.*, 2003). We have found that Bem1 precisely colocalizes with Cdc42 in cells bearing probes for both proteins (Howell *et al.*, 2012; Wu *et al.*, 2015; Woods *et al.*, 2016). Because these probes also accumulate at sites of cytokinesis, and cells often polarize next to previous division sites, it can be difficult to distinguish whether a concentrated signal represents new polarization or a remnant from the previous cell division. To unambiguously distinguish these events, we used *rsr1*Δ strains, where polarity site location is independent of the previous cytokinesis site (Bender and Pringle, 1989). We note that Rsr1 can affect the timing of polarity establishment relative to a point called Start in G1 (Lee *et al.*, 2015; unpublished results). Cells expressing pairs of probes were synchronized by pheromone arrest–release and imaged on slabs at 45-s intervals. Although it is possible that synchronization could affect the precise timing of events, in several cases imaging unsynchronized cells at lower temporal resolution yielded results consistent with those reported below. Example time series are shown in Figure 1, A–C.

Polarity establishment is regulated by G1 cyclin/cyclin-dependent kinase (CDK) complexes (Gulli *et al.*, 2000; Howell and Lew, 2012). CDK activation triggers cell-cycle commitment at Start. We initially compared the dynamics of polarization relative to Start, which can be tracked by monitoring the nuclear export of the yeast Rb analogue Whi5 (Costanzo *et al.*, 2004; de Bruin *et al.*, 2004). Start coincides with the time when 50% of the Whi5 probe exits the nucleus (Doncic *et al.*, 2011). We determined the timing of Start using the customized image analysis tool *ROI_TOI* (see *Materials and Methods*). Previous studies generally treated morphogenetic events in a binary manner (e.g., scoring the percent of cells that have or have not polarized, that have or have not assembled septin rings, or that have or have not budded). Similarly, we visually scored the time of polarization of each probe based on the first detectable concentration of probe at the incipient bud site (Figure 1, A–C). Cells can in some cases initially develop multiple polarity sites or relocate a polarity site (Chen *et al.*, 2012; Howell *et al.*, 2012), complicating the question of when to call initial polarization; for simplicity, we excluded those cells from our analysis.

Based on visual binary scoring, the onset of polarization for Bem1, Sec4, and Cdc3 was on the average 10–12 min after Start, with considerable cell-to-cell variability in this interval (Figure 1, A–C). In addition, different probes appeared to polarize at different rates. To allow more quantitative comparisons of morphogenetic events in individual cells, we adopted a "polarization metric" based on the coefficient of variation (CV) in pixel intensity for a given probe within each cell (see *Materials and Methods* for details). If the probe is uniformly distributed, all pixels have similar intensity and the CV is low, whereas if the probe is highly polarized, a subset of pixels have much higher intensity than the rest and the CV is higher. We found that for several probes the CV was reliably consistent with both visual scoring of the degree of polarization and measurement of the local probe intensity at the polarity site (Supplemental Figure S1). Based on the CV traces, Bem1 and Sec4 became concentrated rapidly, whereas Cdc3 polarized much more gradually (Figure 1, A–C).

Relative timing of polarity establishment, secretory polarization, and septin ring assembly

To better understand the relative timing of events in each cell, we examined cells bearing either a Cdc3 or a Sec4 probe together with a Bem1 probe (Figure 1, D and E). Sec4 polarization reproducibly occurred within 1 min of Bem1 polarization, whereas Cdc3 polarization timing was more variable. In some cells, initial Sec4 accumulation preceded visible Bem1 accumulation by one time point. As the abundance of Sec4 is significantly higher than that of Bem1 (Supplemental Figure S2), it may be that this small difference stems from the better visual detection threshold for Sec4 than for Bem1. We conclude that the initial concentration of Bem1 triggers immediate actin cable orientation toward that site, leading to delivery of Sec4-loaded vesicles within 1 min or less.

The interval between first detection of Bem1 and Cdc3 was more variable than that between Bem1 and Sec4 (SD = 1.5 vs. 0.7 min; $a < 0.01$ by *F*-test) (Figure 1F). This observation suggests that polarity

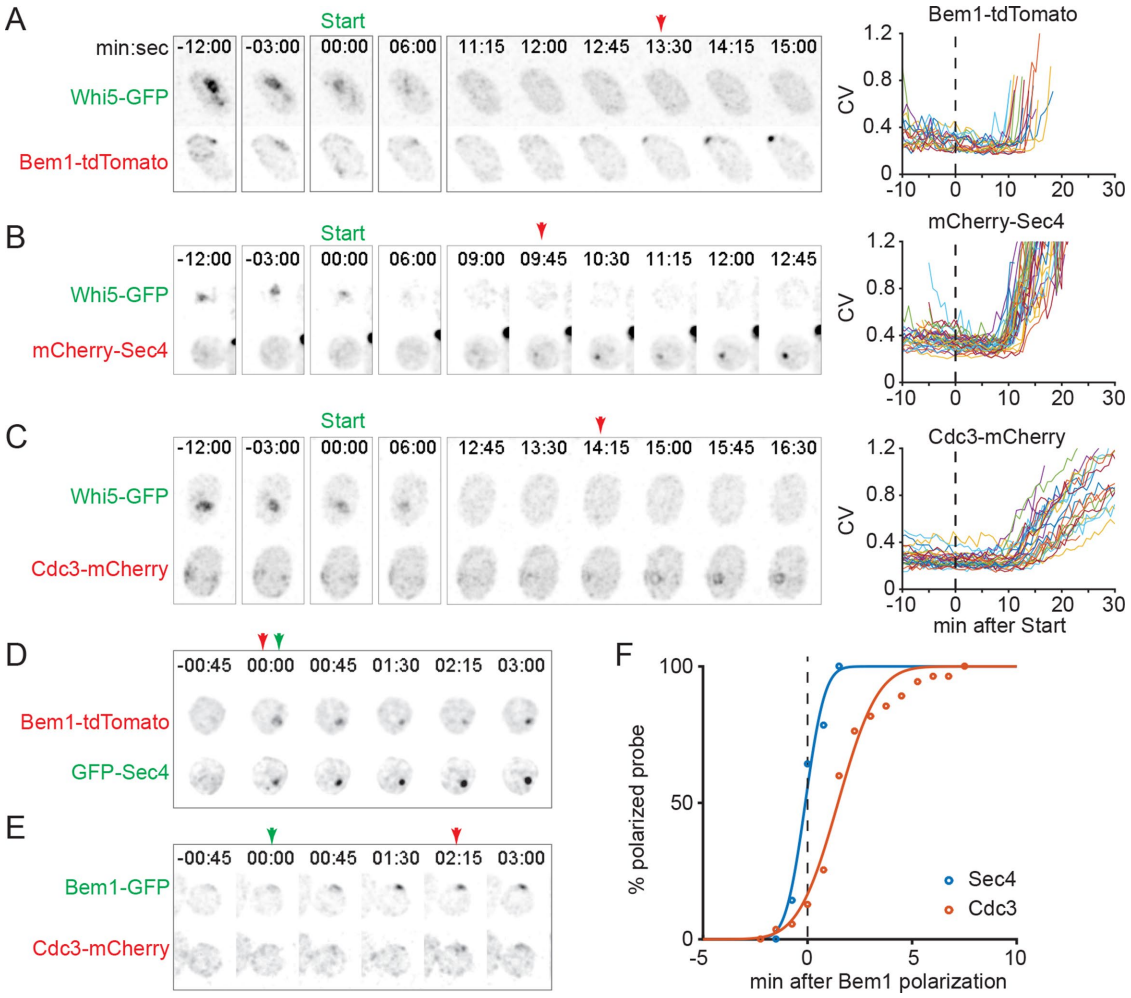

FIGURE 1: Timing and dynamics of polarity establishment, polarized secretion, and septin assembly. Inverted maximum projection montages of illustrative wild-type haploid cells bearing the indicated probes following alpha-factor arrest–release at 24°C. "Start" indicates the time of 50% Whi5 exit from the nucleus, and arrows indicate the first visual detection of probe polarization. (A–C) Polarization dynamics of the polarity scaffold protein Bem1-tdTomato (DLY19233; $n = 17$ cells), the secretory vesicle–associated Rab mCherry-Sec4 (DLY22693; $n = 32$ cells), and the septin subunit Cdc3-mCherry (DLY20258; $n = 28$ cells), all shown relative to the cell cycle Start ($t = 0$) marker Whi5-GFP in the same cell. Probe clustering was quantified using the CV of pixel intensity in each cell; colors indicate different cells. (D, E) Example cells showing GFP-Sec4 (DLY17282) or Cdc3-mCherry (DLY17117) polarization timing relative to Bem1-tdTomato or Bem1-GFP, respectively ($t = 0$). (F) Cumulative probe polarization timing relative to Bem1 in cells from D and E. Dots indicate percent of cells that had polarized the probe by the indicated time. Lines indicate fitted cumulative normal distributions ($n = 31$ cells for Sec4; $n = 51$ cells for Cdc3).

establishment is the only requirement for actin orientation, whereas factors other than polarity establishment also regulate initial septin accumulation.

Effect of delaying vesicle delivery on the dynamics of septin accumulation

Previous work suggested that actin polarization could impact septin ring assembly in at least two different ways. First, a transmembrane protein, Axl2, was identified as a regulator of septin organization (Gao *et al.*, 2007). As Axl2 is delivered to the polarity site on secretory vesicles, actin-targeted secretion could play a role in promoting septin accumulation. Second, it was proposed that the septin-free membrane inserted at the polarity site by vesicle fusion was instrumental in creating the "hole" in the middle of the septin ring (Okada *et al.*, 2013). This hypothesis would explain how a clustered patch of polarity factors could generate a ring (as opposed to a patch) of septins.

To test these ideas, we investigated what effect delaying vesicle delivery would have on septin accumulation (which does not distinguish whether the septins assemble in a ring or other morphology) and septin ring morphology. To that end, we inactivated the formin Bni1, responsible for initial actin cable polarization, using temperature-sensitive *bni1-116* cells (Kadota *et al.*, 2004). Because Bni1 also plays a role during cytokinesis, cells were grown at a permissive temperature and allowed to complete cytokinesis during pheromone-mediated G1 arrest before they were released from the arrest and imaged at the restrictive temperature (37°C). As shown previously (Woods *et al.*, 2016), accumulation of Sec4 at the polarity site was delayed in *bni1-116* mutants by 5.8 min on the average (Figure 2A). However, we found that initial accumulation of Cdc3 occurred with similar timing in wild-type and *bni1-116* cells at 37°C (Figure 2B). As a consequence, the relative order of initial Sec4 and Cdc3 accumulation was reversed in *bni1-116* cells from that in wild-type

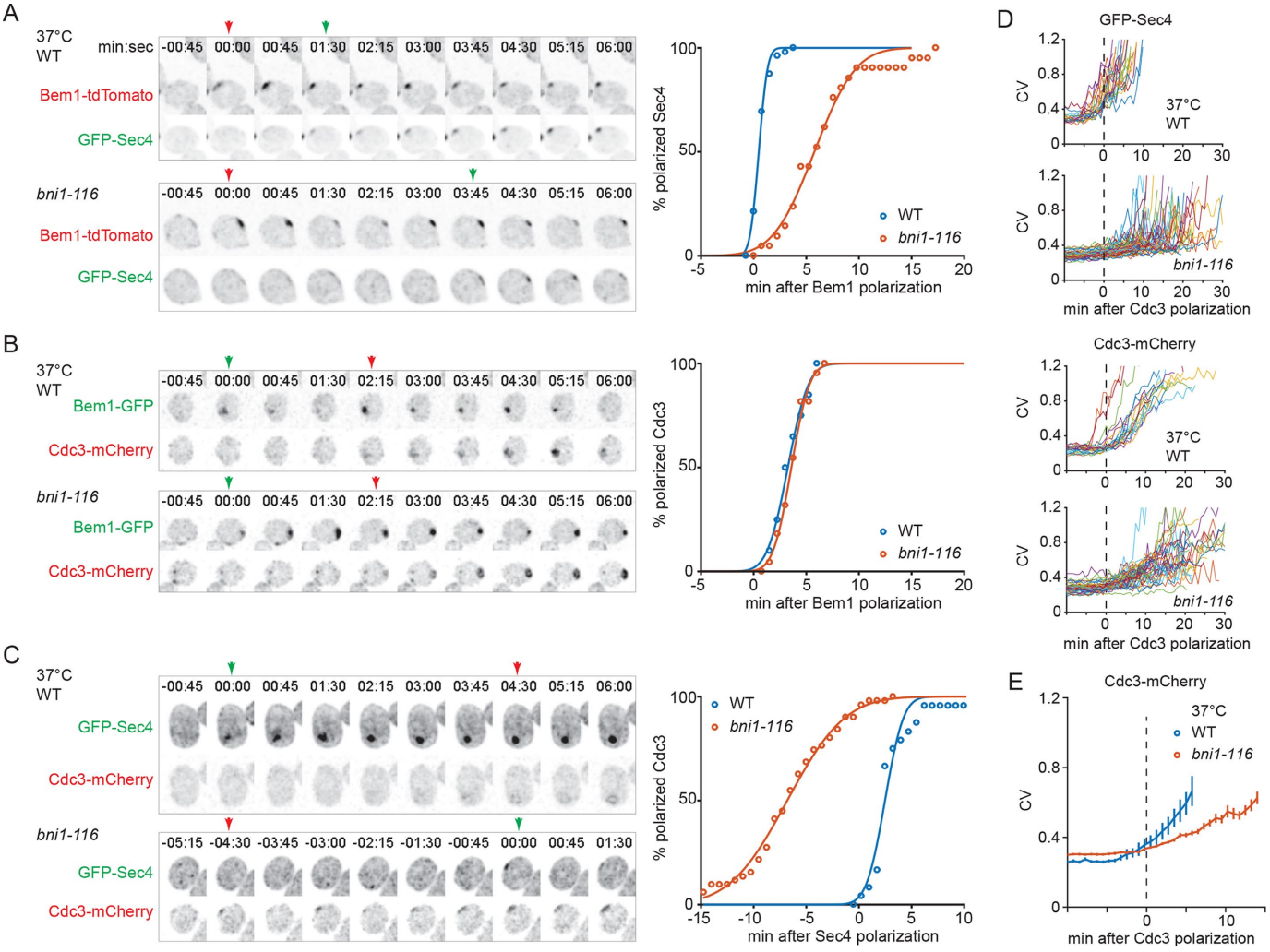

FIGURE 2: Effect of Bni1-nucleated actin cables on septin assembly. Inverted maximum projection montages of wild-type or *bni1-116* haploid cells following alpha-factor arrest at 24°C and then release at 37°C. (A) GFP-Sec4 polarization timing relative to Bem1-tdTomato is delayed in *bni1-116* (DLY20272; $n = 21$) compared with wild-type (DLY17282; $n = 56$) cells. (B) Cdc3-mCherry polarization timing relative to Bem1-GFP is the same in *bni1-116* (DLY20904; $n = 22$) and wild-type (DLY17117; $n = 22$) cells. (C) Relative timing of Cdc3-mCherry and GFP-Sec4 polarization is flipped in *bni1-116* (DLY21105; $n = 51$) compared with wild-type (DLY22546; $n = 24$) cells. (D) Polarization dynamics measured by the CV of pixel intensity of GFP-Sec4 and Cdc3-mCherry in *bni1-116* cells compared with wild-type cells; same cells as in C. (E) Mean ± SEM polarization dynamics of Cdc3-mCherry from D plotted on the same graph for direct comparison of wild-type and *bni1-116* cells.

cells (Figure 2C). Thus, the onset of septin recruitment does not seem to depend on polarized vesicle delivery.

Although the initial timing of septin recruitment was unaffected by the absence of actin cables, *bni1-116* mutant cells displayed reduced and more variable rates of septin accumulation in the period following initial appearance of septins (Figure 2, D and E). This is consistent with the idea that Axl2 (Gao *et al.*, 2007), and possibly other factors delivered on actin cables, assist in the gradual and sustained recruitment of septins to the polarity site (or the bud neck once the bud is formed).

To assess whether vesicle delivery was important for the assembly of septins into a ring rather than a patch, we examined those cells in which we could obtain en face images of assembling septin structures. In both wild-type cells and *bni1-116* mutants, septins first appeared as uneven spots (Supplemental Figure S3). These early-stage septin assemblies have been referred to as uneven or discontinuous septin rings (Chen *et al.*, 2011) or septin clouds (Iwase *et al.*, 2006). In wild-type cells, a strong Sec4 focus was always present by the time that septins became visible, and (consistent with the idea that vesicle delivery creates a septin-free central zone) the early-arriving septins often appeared to populate the annulus surrounding the Sec4 spot (Supplemental Figure S3). In *bni1-116* mutants, similar ringlike septin morphologies could sometimes be observed without any obvious Sec4 spot in the middle, but the morphology of the early septin structure was rather more dynamic than in wild-type cells (Supplemental Figure S3), as noted previously for septins in *Sec4* mutants (Okada *et al.*, 2013). This may indicate that a ringlike configuration can develop even without targeting of vesicles to the center. However, lack of Sec4 accumulation simply indicates that vesicles do not accumulate there, and it is still possible that some number of vesicles are fusing in the center. Septins did form full rings in *bni1-116* mutants, and ring diameters were similar in wild-type and *bni1-116* cells (Supplemental Figure S3D). Thus, the early polarized vesicle delivery mediated by Bni1 does not appear to be required for septins to assemble a ring with a hole in the middle.

In the course of these experiments, we noticed that the interval between Bem1 polarization and initial septin recruitment was longer at 37°C (average 3.2 min) than at 24°C (average 1.5 min; compare Figure 1F with Figure 2B). For some cells at 37°C, there was a delay of several minutes between polarity establishment and detectable septin accumulation, which is consistent with previous reports based on cells at 30°C (Chen *et al.*, 2012; Howell *et al.*, 2012; Merlini *et al.*, 2015). If polarity factors are the only requirement for initiation of septin assembly, then what is the basis for this delay?

Timing of septin accumulation

One possible explanation for the variability in septin assembly following polarity establishment is that there is an additional requirement, beyond polarity establishment per se, for septin recruitment to the polarity site. As cells progress through the cell cycle, there is an increase in CDK activity, and we speculated that the CDK might "prime" septins or septin regulators for subsequent recruitment. This hypothesis makes the prediction that if polarization were to be delayed until after priming had taken place, then septin assembly would follow immediately upon polarization.

To test this hypothesis, we used the reversible temperature-sensitive *cdc24-4* allele (Sloat *et al.*, 1981). Cdc24 encodes the GEF for Cdc42 (Zheng *et al.*, 1994), and at 37°C, *cdc24-4* mutants fail to establish polarity but proceed with the cell cycle until G2 (Lew and Reed, 1995). We synchronized *cdc24-4* mutants in G1 by pheromone arrest–release at 24°C and shifted them to 37°C for 90 min ("delayed" treatment) or, as a control, for only 7 min. During incubation at 37°C, cells grew in a depolarized manner and progressed through the cell cycle (Figure 3A). Upon shift down to 24°C, these cells polarized Bem1, assembled septin rings, and formed buds (Figure 3B). Bem1 dynamics upon shift down were similar in control and delayed cells (Supplemental Figure S4). Strikingly, initial septin recruitment was advanced and there was no longer any delay relative to Bem1 recruitment in the cells that had been incubated at 37°C for 90 min, whereas the delay remained in the control cells (Figure 3, B and D). In addition to the onset of septin assembly being advanced, the rate of Cdc3 accumulation in individual cells was increased in the *cdc24-4* cells in the "delayed" group, as confirmed by averaged data on the rates of septin accumulation (Figure 3E). Interestingly, after the initial ~3 min, the increased accumulation rate decreased and appeared similar to that in the wild type for at least 12 min. In many of the "delayed" cells, septin recruitment preceded detectable Bem1 polarization, suggesting that under these conditions even very low levels of polarity factors suffice to recruit septins efficiently from the cytoplasm.

Our findings are consistent with the hypothesis that a septin-priming event takes place as the cells proceed through the cell cycle. However, it could be that increased cell size, protein amount, or other physiological changes in response to prolonged incubation at a higher temperature, rather than cell cycle progression, were responsible for the subsequent accelerated septin recruitment to the polarity site. To assess the need for cell cycle progression, we repeated the experiment using strains bearing both *cdc24-4* and a temperature-sensitive *cdc28-13* mutation (Reed, 1980). Cdc28 encodes the major cell cycle CDK in yeast (Morgan, 2007). *cdc28-13* mutants remain arrested in G1 during the 90 min incubation at 37°C and do not progress through the cell cycle. Shift-down of *cdc28-13 cdc24-4* cells accelerated septin recruitment, but to a lesser degree than shift-down of *cdc24-4* cells (Figure 3, C and D), suggesting that septins are primed for recruitment to the polarity site by a process that depends (at least in part) on CDK activity. Furthermore, there was no apparent correlation between cell size and the interval between Bem1 polarization and initial septin recruitment (Figure 3F), so the increased cell size per se does not explain the advanced recruitment in the "delayed" *cdc24-4* cells. We also noticed that the septin rings assembled by *cdc24-4* "delayed" cells were larger than those in control cells (Figure 3, B and G). There was a positive correlation between septin ring diameter and cell size (Figure 3H), but long-term imaging of the septin ring size of the same (large) cells showed that they made smaller rings in subsequent cell cycles (Figure 3, I and J), suggesting that increased ring diameter was not simply a consequence of increased cell size. These findings suggest that differences in the relative timing of septin priming and polarization can lead to abnormalities in septin ring size, and possibly in septin organization.

Timing of bud emergence

Next, we examined the timing of bud emergence, whose early stages were difficult to see using DIC microscopy. To facilitate accurate detection of bud emergence, we collected *z*-stacks of cells expressing a plasma membrane probe based on the N-terminal 28 residues of Psr1 (Figure 4A; Kuo *et al.*, 2014). In favorable instances where bud emergence occurred perpendicular to the imaging *z*-axis, bud emergence was seen to involve an acceleration of local cell expansion, which could be captured on kymographs using a custom software *BudTrack* (*Materials and Methods*), allowing us to call a time of bud emergence (Figure 4A). However, this was more difficult in cases where buds formed at oblique angles or the cell rotated due to the growth of a nearby cell. To allow consistent determination of initial bud emergence, we developed an "Automated Fitting" mode in *BudTrack* to create a continuous three-dimensional (3D) surface rendering of the cell so that bud formation could be observed from any angle (*Materials and Methods*), as illustrated in Figure 4B. Bud emergence involves a change in the rate of local outgrowth (Figure 4, A and C). On the average, bud emergence occurred 24 min after Start (Figure 4D). Population-level data indicated that the timing of bud emergence was offset from and more variable (SD = 7.4 min) than the onset of polarized secretion (SD = 1.7 min; Figure 4, D and E).

A closer look at the cell outline kymograph and bud volume change also highlighted the very limited local growth during the interval from polarized secretion to bud emergence as compared with the more rapid subsequent growth after bud emergence (Figure 4, A and C). If polarized secretion delivered bud-building material to the polarity site at a constant rate and that rate translated in a linear manner to the rate of growth, then it should not have taken ~9 min to detect a change in cell shape (compare the bud size at $t = 0$, 6:45, and 13:30 in Figure 4B). The lack of obvious growth at the polarized secretion site around the time of bud emergence is consistent with previous studies that reported a decrease in growth rate around the same time (Di Talia *et al.*, 2007; Goranov *et al.*, 2009).

One possibility is that, as suggested for septin priming, other CDK-dependent events may be needed to promote bud emergence. CDK activity is known to promote transcriptional induction of cell-wall genes such as the glucan synthase Fks1 (Mazur *et al.*, 1995; Ram *et al.*, 1995), suggesting that polarized secretion might cause different cell-wall modifications before and after CDK-induced transcriptional changes. Thus, the delay between the onset of polarized secretion and the emergence of a bud could reflect the time it takes to promote synthesis of cell-wall components. A prediction of this hypothesis is that if polarity establishment were delayed until later in the cell cycle (when the relevant genes were

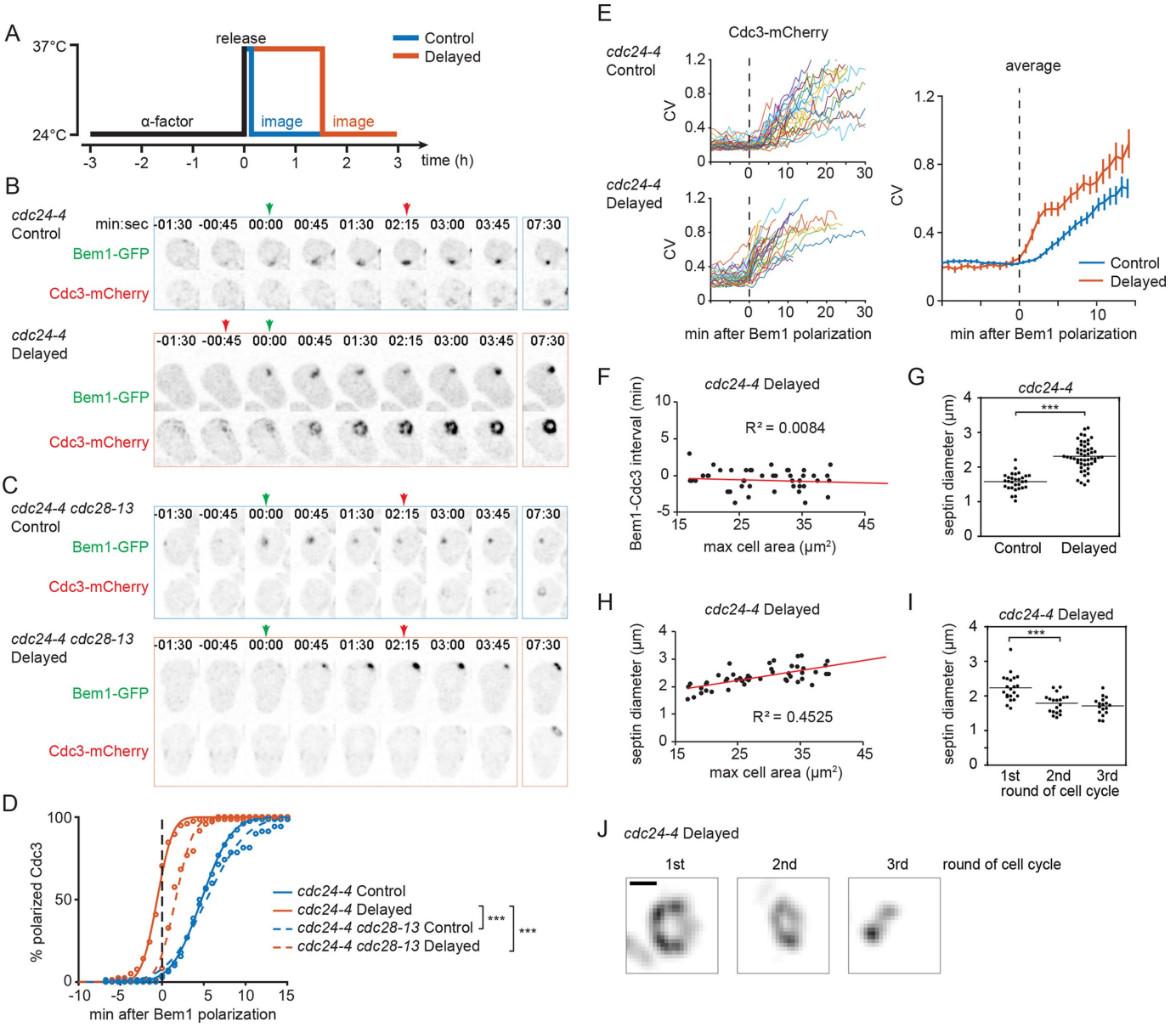

FIGURE 3: Effect of delayed polarity establishment on septin assembly. (A) Schematic illustration of the experimental procedure. (B, C) Illustrative inverted maximum projection montages of cells comparing Cdc3-mCherry polarization timing relative to Bem1-GFP ($t = 0$) in (B) *cdc24-4* (two independent isolates, DLY21169 and DLY22202) control and delayed cells, and (C) *cdc24-4 cdc28-13* (two independent isolates, DLY22061 and DLY21995) control and delayed cells. (D) Cumulative Cdc3 polarization timing in cells from B and C (control $n = 63$ cells and delayed $n = 78$ cells for *cdc24-4* across isolates; control $n = 70$ cells and delayed $n = 73$ cells for *cdc24-4 cdc28-13* across isolates). (E) Polarization dynamics of Cdc3-mCherry in individual cells (left) and mean ± SEM (right) in *cdc24-4* delayed and control cells from B. (F) Correlation of cell size and the interval between Bem1-GFP and Cdc3-mCherry polarization in cells from B. Cell size was measured as cell area in maximum projection images at the time point of Bem1-GFP polarization. (G) Septin ring diameter, measured 7.5 min after polarity establishment, in *cdc24-4* delayed and control cells from B. (H) Correlation of cell size and septin ring diameter, measured 7.5 min after polarity establishment, in *cdc24-4* delayed cells from B. (I) Septin diameter, measured 7.5 min after polarity establishment, over three sequential cell cycles at 24°C following delayed treatment (DLY21169; $n = 20$, 19, and 17). The same cells were measured in each cell cycle. (J) Illustrative inverted maximum projection images of septin rings in the same cell through sequential cell cycles as in I. Scale bar, 1 μm. En face images for the first and second cell cycles, and side view image for the third cell cycle. ***$p < 0.001$ by two-tailed *t* test assuming unequal variance.

expressed), then bud emergence would follow closely after secretory polarization.

To test this hypothesis, we used a protocol similar to the one described above to analyze the timing of septin recruitment (Figure 3A). Synchronized *cdc24-4* mutants were shifted to 37°C to allow cell cycle progression without polarity establishment, and the timing of Sec4 polarization and bud emergence was monitored following shift-down to 24°C. Unlike the delay between polarity establishment and septin recruitment, the delay between Sec4 polarization and bud emergence was unaffected by delaying polarity establishment

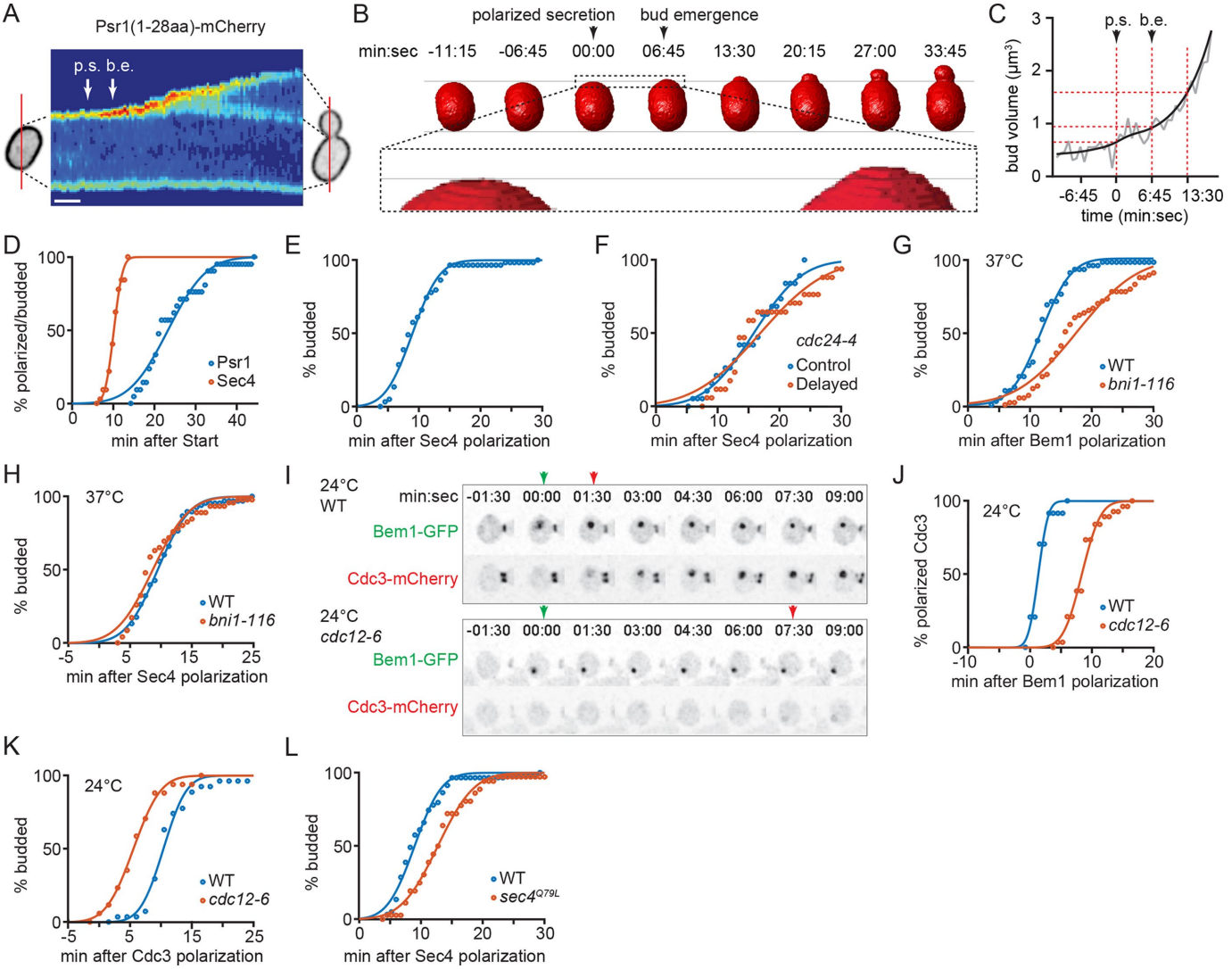

FIGURE 4: Effects of delayed polarity establishment, actin cable nucleation, and septin assembly on the timing of bud emergence. (A) Kymograph of a plasma membrane marker, Psr1(1-28aa)-mCherry, from a single *z* plane of an illustrative cell (DLY20823), where p.s. is onset of polarized secretion determined by visual calling based on the GFP-Sec4 channel (not shown) and b.e. is bud emergence determined by *BudTrack* as illustrated in B. Scale bar = 7.5 min. Color represents signal intensity, red being the brightest signal and dark blue being the dimmest signal. (B) 3D reconstructed cell surface used to determine the timing of bud emergence in the cell from A. After secretion becomes polarized (0:00) but before bud emergence can be detected by eye (6:45), there is very little change in the morphology of the mother cell. (C) Bud growth rate speeds up after bud emergence as estimated by fitted bud volume for the cell from A (raw data in gray and smoothed data in black). Bud volume before bud emergence is greater than 0 due to noise in fitting an ellipsoid to the bud. The noise stems from *BudTrack* recognizing a small region of the mother-cell contour that is outside of the ellipse fitted to the mother cell. (D) Cumulative mCherry-Sec4 polarization (DLY22693; $n = 32$) and bud emergence (DLY20784; $n = 21$) timing relative to Start in wild-type haploid cells following alpha-factor arrest–release at 24°C. (E) Cumulative bud emergence timing relative to GFP-Sec4 polarization in wild-type haploid cells following alpha-factor arrest–release at 24°C (DLY20823; $n = 58$). (F) Cumulative bud emergence timing relative to GFP-Sec4 polarization in *cdc24-4* control ($n = 19$) and delayed ($n = 17$) cells following treatment illustrated in Figure 3A (two independent isolates, DLY21132 and DLY21996). (G) Cumulative bud emergence timing relative to Bem1-GFP polarization in wild-type (DLY18870; $n = 41$) and *bni1-116* (DLY20663; $n = 62$) cells following alpha-factor arrest at 24°C and release at 37°C. (H) Cumulative bud emergence timing relative to GFP-Sec4 polarization in wild-type (DLY20823; $n = 68$) and *bni1-116* (DLY20887; $n = 46$) cells following alpha-factor arrest at 24°C and release at 37°C. (I) Illustrative inverted maximum projection montages of cells, comparing Cdc3-mCherry polarization timing relative to Bem1-GFP in wild-type (DLY17117) and *cdc12-6* (DLY22350) mid-log phase cells grown at 24°C. (J) Cumulative Cdc3-mCherry polarization timing relative to Bem1-GFP polarization for cells from I ($n = 24$ cells for DLY17117; $n = 57$ cells for DLY22350). (K) Cumulative bud emergence timing relative to Cdc3-GFP in wild-type (DLY22470; $n = 27$) and *cdc12-6* (DLY22469; $n = 17$) asynchronous cells grown at 24°C. (L) Cumulative bud emergence timing relative to GFP-Sec4 polarization in wild-type (DLY20823; $n = 58$) and $Sec4^{Q79L}$ (DLY22528; $n = 36$) cells following alpha-factor arrest–release at 24°C.

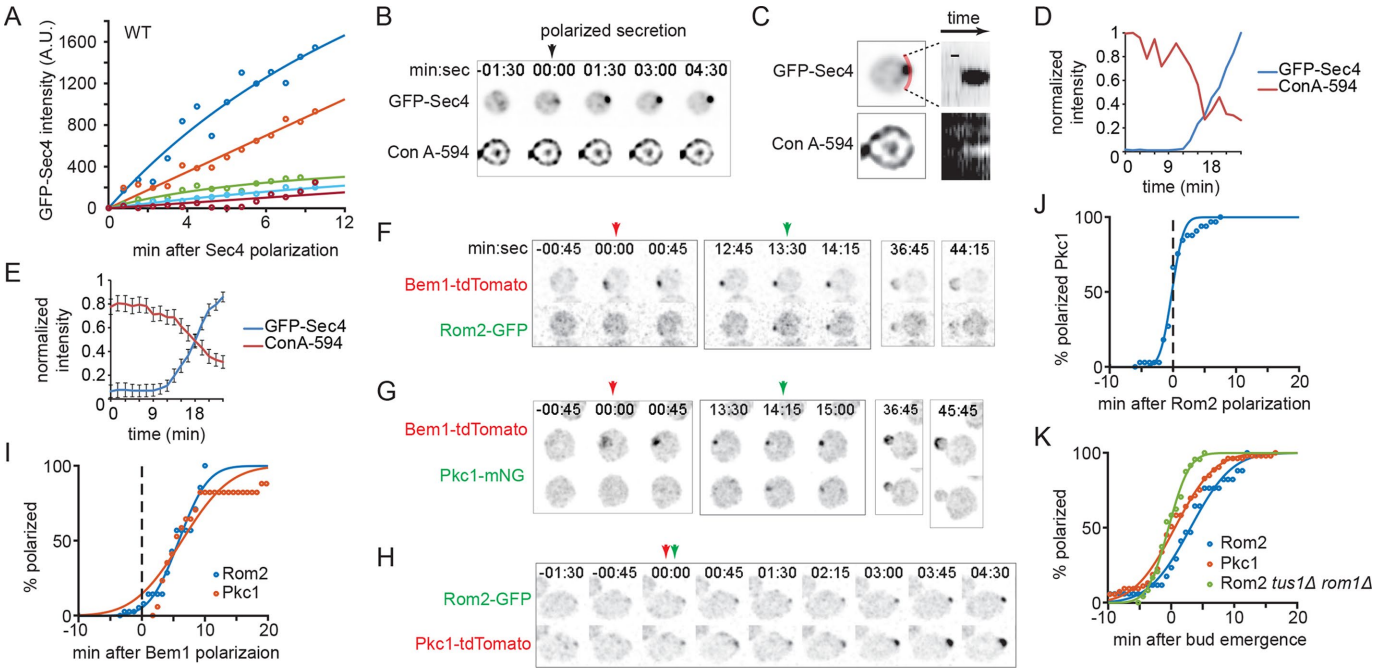

FIGURE 5: Timing of cell-wall modification and Rho1 activation. (A) Accumulation of GFP-Sec4 at the polarity site in five example cells using the analysis tool *Vicinity*. (B) Illustrative inverted maximum projection montages of a cell bearing GFP-Sec4 prestained with Con A-594 to label wall mannoproteins (DLY9880). Polarized secretion is accompanied by local diminution of Con A signal. (C) Single *z*-plane line-scan kymograph of the cell from B over time. Scale bar = 6 min. (D) GFP-Sec4 and Con A-594 intensity at the polarity site of the cell in B. (E) GFP-Sec4 and Con A-594 intensity (mean ± SEM) at the polarity site (DLY9880; $n = 16$). (F, G) Illustrative inverted maximum projection montages of cells bearing Rom2-GFP (DLY22105) or Pkc1-mNeonGreen (DLY22185) and Bem1-tdTomato following alpha-factor arrest–release at 24°C. (H) Illustrative inverted maximum projection montages of cells bearing Rom2-GFP and Pkc1-tdTomato (DLY22247) following alpha-factor arrest–release at 24°C. (I) Cumulative timing of probe polarization for the cells from F, G ($n = 37$ cells for Rom2; $n = 17$ cells for Pkc1). (J) Cumulative timing of probe polarization for the cells from H ($n = 33$ cells). (K) Cumulative polarization timing of Rom2-GFP (DLY22000; $n = 17$) or Pkc1-mNeonGreen (DLY22079; $n = 53$) in wild-type cells and Rom2-GFP in *rom1Δ tus1Δ* (DLY22267; $n = 24$) cells relative to bud emergence following alpha-factor arrest–release at 24°C. There is no significant difference between the three data sets by analysis of variance.

(Figure 4F), indicating that the timing of bud emergence is not explained by CDK activity or cell cycle stage.

What, then, is the basis for the significant and variable delay between secretory polarization and bud emergence? We assume that polarized secretion initiates a series of changes in cell-wall composition that are required for bud emergence. If these modifications are rate-limiting for bud emergence, then delaying secretory polarization should lead to a corresponding delay in bud emergence. To assess whether that was the case, we used *bni1-116* mutants to delay secretory polarization. Mutant and wild-type control cells were synchronized at a permissive temperature and released from G1 arrest at 37°C. Relative to polarity establishment, bud emergence was delayed in *bni1-116* mutants by 5.8 min on the average, comparable to the delay of polarized secretion in the mutants (Figures 2A and 4G), indicating that actin polarization is rate-limiting for bud emergence. Moreover, the interval between Sec4 polarization and bud emergence was similar in *bni1-116* and wild-type control cells (Figure 4H), suggesting that no parallel pathways or priming effects are responsible for the timing of bud emergence.

Nevertheless, as reported in Figure 2E, incubating *bni1-116* cells at 37°C lowered the accumulation rate of septins, in addition to delaying early polarized secretion. It is therefore possible that delayed bud emergence timing in *bni1-116* cells was a result of altered septin assembly dynamics. Serendipitously, we discovered that *cdc12-6* septin mutants (Adams and Pringle, 1984) delayed septin ring assembly by 7 min relative to polarity establishment, even at the permissive temperature, allowing us to ask whether septin assembly contributes to the timing of bud emergence (Figure 4, I and J). Delayed septin polarization in *cdc12-6* was not accompanied by a commensurate delay of bud emergence (Figure 4K), suggesting that septin ring assembly is not a major factor in initial bud formation.

To ask whether polarized secretion itself affects the timing of bud emergence, we specifically perturbed vesicle fusion. Sec4 GTP hydrolysis is thought to be rate-limiting for vesicle fusion with the plasma membrane, based in part on observations with a mutant that slows GTP hydrolysis, Sec4^{Q79L} (Walworth *et al.*, 1992; Donovan and Bretscher, 2015). Indeed, cells bearing GFP-Sec4^{Q79L} as the sole source of Sec4 exhibited a delay in bud emergence relative to secretory polarization (Figure 4L). Together, these findings suggest that the timing of bud emergence is governed by the onset of polarization of secretion.

Timing of cell-wall modification

We noticed that the Sec4 signal (measured as described under *Materials and Methods*), and hence presumably the number of secretory vesicles at the polarity site, increased gradually with time in individual cells (Figure 5A). As Sec4 signal dissipates after vesicle fusion (Donovan and Bretscher, 2015), this surprising observation suggests that for several minutes after polarity is established, delivery of vesicles to the polarity site outpaces their fusion with the plasma membrane. This observation is consistent with older electron microscopy literature showing clusters of secretory vesicles

backed up at the sites of emerging buds (Mulholland *et al.*, 1994). A possible explanation for the accumulation of secretory vesicles is that vesicles do not initially fuse when they reach the polarity site, but rather wait for some later signal before fusing with the plasma membrane. If that were the case, it could explain the delay between vesicle accumulation and bud emergence.

To assess when vesicle fusion occurs, we examined the timing of cell-wall modification. The cell wall is constructed primarily of cross-linked glucan polymers (the major load-bearing elements) and heavily glycosylated cell-wall mannoproteins ("mannans," the major permeability determinants). Chitin (a polymer of N-acetyl glucosamine) is a minor constituent that is enriched in a ring at the base of the bud and is thought to provide mechanical protection to the mother-bud neck (Schmidt *et al.*, 2003). Glucan and chitin polymers are extruded by transmembrane synthases that use cytoplasmic UDP-glucose or UDP-GlcNAc as polymerization substrates (Orlean, 2012).

Mannans as well as glucan-remodeling enzymes are delivered to the cell wall via the secretory pathway. Mannans can be detected by the mannose-binding lectin concanavalin A (Con A). When fluorescent Con A is incubated with cells, the entire wall becomes fluorescent (Figure 5B). After removal of excess unbound Con A, local breakdown of existing, labeled mannan and insertion of new, unlabeled mannan can be detected as a local decrease in Con A fluorescence (Figure 5, B–E). If vesicles begin fusing as soon as they begin to accumulate at the polarity site, then new mannan insertion should be detected at around the time of Sec4 polarization. Indeed, new mannan insertion began as soon as Sec4 was concentrated at the polarity site (Figure 5, B–E), well before bud emergence. Thus, local cell-wall modification proceeds immediately upon secretory polarization.

If secretion and cell-wall modification begin simultaneously, why is there no detectable change in cell shape for several minutes? Once bud emergence occurs, a similar several-minute interval yields a much more significant expansion of the bud (Figure 4, A–C). Thus, either there is a change in the nature of the cell-wall modification that occurs right before bud emergence, or the same modifications take much longer to alter the shape of the unbudded mother-cell wall than they do to alter the cell wall of a growing bud. Such modification might not be limited to only one component of the cell wall (mannans). In fact, the primary load-bearing component of the cell wall consists of cross-linked glucan polymers, which are synthesized by the integral membrane glucan synthases Fks1 and Fks2. These enzymes are activated by GTP-Rho1 (Drgonova *et al.*, 1996; Qadota *et al.*, 1996), and activation of Rho1 is mediated by the Rho-GEFs Tus1, Rom1, and Rom2 (Levin, 2005). To assess when glucan synthesis might be initiated at the polarity site, we next examined the localization of these GEFs.

A previous study reported that Tus1 and Rom2 localize to the bud neck during cytokinesis, but only Rom2 was detected at the incipient bud site and the growing bud tip, suggesting that Rom2 is involved in bud formation (Krause *et al.*, 2012). In our strain background, deletion of *ROM2* was lethal (Supplemental Figure S5A), while deletion of *ROM1*, *TUS1*, or both was not. Thus, we focused on Rom2. Rom2-GFP was functional as the sole source of Rom2 (Supplemental Figure S5B). Rom2 was localized to polarity sites but surprisingly was only detected ~10 min after Bem1 polarization (Figure 5, F and I). The Rom2-GFP probe is faint (presumably because Rom2 has a lower abundance than the other proteins we imaged), raising the possibility that functionally relevant levels of Rom2 at the polarity site might go undetected. To address that possibility, we sought to image the GTP-Rho1 presumably generated by Rom2.

Previous studies used the Rho1 effector Pkc1 for that purpose (Denis and Cyert, 2005), and we found that Pkc1-mNeonGreen and Pkc1-tdTomato probes were functional (Supplemental Figure S5C) and significantly brighter than Rom2-GFP. As for Rom2, Pkc1 polarization occurred several minutes after Bem1 polarization (Figure 5, G and I) and behaved similarly to Rom2 when imaged in the same cells (Figure 5, H and J). In cells bearing the plasma membrane probe, which allows accurate detection of bud emergence, we found that both Rom2 and Pkc1 cluster at the polarity site shortly before bud emergence (Figure 5K). When Rom2 was the only Rho1 GEF in the cell, its polarization timing was slightly advanced but still similar to Pkc1 polarization timing, and the interval between polarized secretion and bud emergence was comparable to that of the wild type (Figure 5K, Supplemental Figure S6). These data suggest that polarized Rho1-GTP accumulation, and presumably glucan synthesis, only occurs several minutes after the onset of polarized secretion and mannan modification.

Aside from the stable, persistent localization of both Rom2 and Pkc1 at the polarity site around the time of budding, we noticed that in some cells Rom2 and Pkc1 puncta formed and then disappeared at random sites (Supplemental Figure S7). Occasionally, transient puncta colocalized with Bem1, but soon disappeared (except around the time of budding). As Pkc1 is central to the cell-wall integrity (CWI) pathway (Levin, 2005), we speculate that these puncta may represent transitory weak spots in the cell wall that are rapidly repaired following Pkc1 recruitment.

DISCUSSION

Extensive study of the requirements for bud emergence led to a detailed understanding of the underlying mechanism: CDK activation at Start promotes clustering of polarity regulators including Cdc42, which in turn promotes assembly of oriented actin cables and a septin ring at the polarity site (Howell and Lew, 2012). These cytoskeletal rearrangements lead to polarized secretion of cell-wall proteins and modifying enzymes, as well as localized synthesis of cell-wall polysaccharides, which in turn lead to bud emergence. But how would such a series of reproducible biochemical reactions lead to the observed variability in the timing of these events from cell to cell? To address that question, we examined the relative timing of events at the single-cell level. Whereas polarity establishment reproducibly led to oriented actin-dependent polarization of secretion within 1 min, there was significantly greater variability in the interval between polarity establishment and septin ring formation. Our findings suggest that septins must be "primed" in a CDK-dependent manner before they can be recruited to the polarity site by Cdc42, introducing a delay between polarity establishment and septin recruitment that ensures proper ring formation (Figure 6). There was also a delay between the polarization of secretion and the emergence of a bud, but in this case the timing of bud emergence was nevertheless determined by the timing of polarized secretion. We suggest that an interval of polarized secretion is necessary to weaken the mother-cell wall sufficiently to allow bud emergence, and we identify a key role for Rom2, possibly activated by the CWI pathway, in activating local glucan synthesis to promote bud formation (Figure 6).

CDK-mediated septin priming

As in previous studies (Chen *et al.*, 2012; Howell *et al.*, 2012), we documented the unexplained presence of a delay between polarity establishment and detectable septin recruitment to the polarity site. This delay was dependent on temperature (being longer at 37°C than at 24°C), was severely exacerbated by a *cdc12-6* mutation even at 24°C, and was variable from cell to cell. We found that the

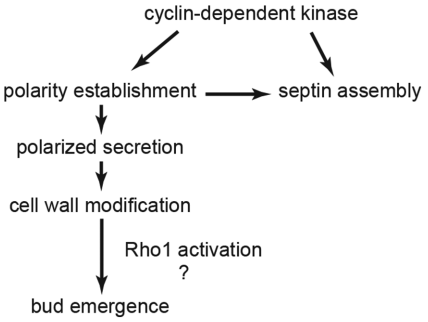

FIGURE 6: Schematic of temporal regulation of morphogenetic events in *S. cerevisiae*. CDK is key to both triggering polarity establishment and priming septins for assembly at the polarity site. Subsequently, secretion becomes focused, leading to immediate local cell-wall modification at the incipient bud site. Over time, the weakening of the cell wall leads to bud emergence, which coincides with the time of Rho1 activation. We speculate that gradual cell-wall weakening leads to eventual activation of Rho1 by Rom2 to promote glucan synthesis.

delay could be eliminated if cells were allowed to progress further in the cell cycle before initiating polarity establishment. The dynamics of polarity protein clustering were unaffected by this protocol (Supplemental Figure S4), indicating that the effect is specific to septin assembly. Elimination of the delay required CDK activity and was accompanied by more rapid septin accumulation at the polarity site. These data suggest that CDK activity "primes" septins (either directly or via regulators) to facilitate their recruitment by polarity factors. Studies in various fungi have suggested that CDKs directly phosphorylate septins and/or septin regulators, providing a potential mechanism for septin priming (Cvrckova *et al.*, 1995; Tang and Reed, 2002; Gladfelter *et al.*, 2005; Sinha *et al.*, 2007; Egelhofer *et al.*, 2008; Gonzalez-Novo *et al.*, 2008; Li *et al.*, 2012).

Notably, the septin rings formed under higher CDK activity had visibly different morphologies. As with control rings, the septins were initially recruited to form a discontinuous set of spots around the circumference of a circle, with subsequently recruited septins filling in the gaps to generate a smooth circle. But the discontinuous stage lasted longer, the ring grew to an abnormally large diameter, and in some cases sections of the initial ring later disappeared as the ring shifted laterally (Supplemental Movies S1 and S2). These observations suggest that higher CDK activity might negatively impact the assembly of a proper ring. Aberrant septin ring formation could possibly result from the accelerated septin assembly.

Quantification of septin recruitment revealed that rings formed under higher CDK activity accumulated septins in a biphasic manner, with an early phase of rapid septin accumulation followed by continued recruitment at the normal rate. It remains unclear what triggers this switch in septin accumulation rate.

Relation between actin and septin assembly

Actin depolymerization causes defects in septin ring formation (Kadota *et al.*, 2004; Kozubowski *et al.*, 2005; Iwase *et al.*, 2006), and this has been proposed to reflect roles for actin-mediated vesicle traffic in creating a hole in the middle of a septin patch (Okada *et al.*, 2013) or in delivering septin regulators to the neck (Gao *et al.*, 2007). To dissect the role of actin cables in the dynamics of septin assembly, we employed a conditional allele of the yeast formin Bni1, *bni1-116*, that delays the onset of polarized secretion without affecting Cdc42 polarization. Exploiting *rsr1Δ* mutants to find en face views of assembling septin rings, we found no obvious effect of *bni1-116* on septin ring morphology or diameter (Supplemental Figure S3). However, the septin accumulation rate was dampened in a subset of *bni1-116* cells, consistent with the idea that secretory vesicles deliver factors such as Axl2 that facilitate septin recruitment.

Polarized secretion is rate-limiting for bud emergence

F-actin and exocytosis are both required for bud emergence (Ayscough *et al.*, 1997), but there was a significant delay between the onset of polarized secretion and bud emergence. This raised the possibility that the timing of bud emergence might be influenced by parallel processes such as a rise in CDK activity or the assembly of a septin ring. However, our findings do not support that hypothesis. Using different approaches to perturbing exocytosis, we found that delaying the polarized delivery or the fusion of secretory vesicles caused a commensurate delay in bud emergence. This finding indicates that polarized secretion initiates a series of events that culminate 9 min later in bud emergence.

Delay between secretory polarization and bud emergence

To understand why it takes 9 min to start budding, we examined the timing of cell-wall modification. Local modification of mannoproteins began immediately upon secretory polarization. However, we did not detect sustained local activation of the glucan synthesis regulator Rho1 (assessed using the Rho1 effector Pkc1 as a probe) until around the time of bud emergence. The Rho1 GEF Rom2 is known to act downstream of the cell-wall sensors Wsc1 and Mid2 in response to stress that threatens the integrity of the cell wall (Gray *et al.*, 1997; Ketela *et al.*, 1999; Rajavel *et al.*, 1999), and Rom2 also became polarized at around the time of bud emergence. We speculate that the recruitment of Rom2 to the incipient bud site is due to the cumulative cell-wall weakening caused by polarized delivery of wall-degrading enzymes on vesicles. Bud emergence then occurs as turgor pushes against the locally weakened wall, and Rho1 activation provides the additional glucan synthesis necessary to support this morphological change (Figure 6).

An alternative and not mutually exclusive hypothesis regarding the timing of local Rho1 activation stems from previous findings that another Rho1 GEF, Tus1, undergoes CDK-dependent activation in late G1 (Kono *et al.*, 2008). However, we were unable to detect Tus1 at the bud site, cells tolerated the loss of Tus1 and Rom1 with only minor effects on the timing of bud emergence (Supplemental Figure S6), and increased CDK activity did not advance the timing of bud emergence.

During the interval between secretory polarization and bud emergence, cell expansion is undetectable, but once a visible bud has emerged, growth accelerates rapidly. This pause in volume increase is consistent with the previously reported increase in cell density during this time window (Bryan *et al.*, 2010), assuming a constant rate of mass increase in cells. In thin section electron micrographs, the thickness of the cell wall appears greater in the mother cell than in the bud (Sentandreu and Northcote, 1969; Linnemans *et al.*, 1977; Roh *et al.*, 2002). We speculate that a rate of cell-wall modification sufficient to promote growth of the thin-walled bud may take some time to modify the thicker mother-cell wall, accounting for the delay between secretory polarization and bud emergence.

Secretory vesicles accumulate at the bud site

Electron micrographs of cells with very small buds show clusters of secretory vesicles at the incipient bud sites (Mulholland *et al.*, 1994), but the dynamics of vesicle accumulation was unknown. Here we report an increase in the Sec4 signal from the onset of polarized

secretion to around the time of budding, suggesting that the rate of vesicle delivery is greater than that of vesicle fusion, leading to gradual vesicle accumulation. We have shown that secretory vesicles begin to fuse with the plasma membrane as soon as secretion becomes polarized. It remains unclear whether the vesicle delivery and fusion rates change over time and why there was considerable cell-to-cell variability in Sec4 accumulation rate. A similar vesicle cluster, the Spitzenkörper, has been described in many filamentous fungi. In *Ashbya gossypii*, the formation and expansion of the Spitzenkörper is associated with an acceleration in the hyphal growth rate (Kohli *et al.*, 2008). Why it is advantageous to have a cluster of vesicles located behind the growing tip is unclear. It is possible that the Spitzenkörper simply arises from the imbalance of vesicle delivery and fusion rates.

MATERIALS AND METHODS

Yeast strains

All yeast strains used in this study (Supplemental Table S1) are in the YEF473 background (*his3-Δ200 leu2-Δ1 lys2-801$_{amber}$ trp1-Δ63 ura3-52*) (Bi and Pringle, 1996). Genetic alterations (deletions and gene tagging) were introduced into diploid strains by transformation with appropriate PCR products, and desired strains were derived by sporulation and tetrad dissection, with further crossing as needed.

Fluorescent probes, including Bem1-GFP (Kozubowski *et al.*, 2008), Bem1-tdTomato (Howell *et al.*, 2012), GFP-Sec4 (Chen *et al.*, 2012), Cdc3-mCherry (Chen *et al.*, 2011), Cdc3-GFP (Chen *et al.*, 2011), and Psr1(1-28aa)-mCherry (Kuo *et al.*, 2014), were described previously. All proteins are fluorescently tagged at the endogenous locus except GFP-Sec4 and mCherry-Sec4, which are inserted at *URA3* and *LEU2*, respectively. GFP-Sec4^{Q79L} was generated by PCR with primers that carry the mutated sequence, subcloned into pDLB4388 (*pRS306-YeGFP-SEC4 (last 81 bases truncated)*; Schott *et al.*, 2002), digested with *Bsp*E1 to integrate at the *SEC4* locus in a diploid strain, and sporulated to obtain the final strain.

Pkc1-mNeonGreen, Pkc1-tdTomato, and Rom2-GFP are generated by PCR amplification of the fluorophore open reading frames from pDLB4373 (*pNCS-mNeonGreen:nat$_R$*; Allele Biotechnology), pDLB3299 (*pFA6a-tdTomato-HIS3*), and pDLB3524 (*pFA6a-GFP(S65T)-KanMX6*) with 50 base pairs of homology to the C terminus and 3′ UTR regions of the target genes to allow homologous recombination for protein tagging. Correct integration was confirmed by PCR and sequencing.

The temperature-sensitive alleles *bni1-116* (Kadota *et al.*, 2004), *cdc24-4* (Sloat *et al.*, 1981; Kozubowski *et al.*, 2008), *cdc28-13* (Reed, 1980) and *cdc12-6* (Adams and Pringle, 1984; Lee *et al.*, 2002) are also from previous studies. *cdc28-13* was introduced to the YEF473 background by PCR with primers that amplify 604–789 base pairs of *cdc28-13* with additional *Xba*I/*Xho*I sites at the ends using a strain of 15Du background (DLY107; Reed, 1980) as the template. The PCR product was subcloned into pDLB212 (*pRSII306*) using *Xba*I/*Xho*I, digested with *Msc*I to integrate at the *CDC28* locus in a diploid strain, and sporulated to generate a haploid stain, and then the wild-type *CDC28* and *URA3* markers were popped out using 5-fluoroorotic acid selection to obtain the final strain. Correct replacement was confirmed by sequencing and temperature-sensitive phenotype.

The *rom1Δ, rom2Δ,* and *tus1Δ* strains were generated using PCR to amplify drug resistance markers from plasmids pDLB147 (*pRS40N-natMX4*) and pDLB148 (*pRS40H-hphMX4*) with 50 base pairs of homology flanking the open reading frames of the target genes to allow gene deletion by homologous recombination (Baudin *et al.*, 1993). Correct deletion was verified by PCR from genomic DNA.

Live-cell microscopy

Cells were grown to mid–log phase in liquid complete synthetic medium (CSM; MP Biomedicals) containing 2% dextrose at 24°C unless otherwise indicated. Where pheromone arrest–release is indicated, cells were diluted to 0.75×10^7 cells/ml and arrested with 2 µM alpha factor (Genway Biotech) for 3 h, harvested, washed twice, and placed on a slab lacking alpha factor for imaging. Slabs were made of CSM + 2% dextrose solidified with 2% agarose (Denville Scientific), and the coverslip was sealed over the slab with petroleum jelly to prevent evaporation.

All live-cell microscopy was carried out with an Andor Revolution XD spinning-disk confocal microscope (Olympus) with a 100× oil-immersion 100×/1.4 UPlanSApo objective and an Andor Ixon3 897 512 EMCCD camera. *z*-stacks (0.5 µm spacing) of 15 images were acquired at two stage positions every 45 s. Laser power was set to 6–10% for both 488- and 561-nm illumination, with 200 ms exposure and 200 Hz EM gain. Unless otherwise indicated, live-cell microscopy was done at room temperature ranging from 23 to 26°C.

Cell-wall staining with concanavalin A

Mid–log phase cells grown in CSM + 2% dextrose were harvested, resuspended in 50 µg/ml concanavalin A–Alexa Fluor 594 Conjugate (Con A-594; ThermoFisher Scientific) in water, incubated at room temperature for 5 min, and washed with CSM + 2% dextrose twice before being loaded onto an agarose slab for imaging.

Image analysis

Images were deconvolved using SVI Huygens deconvolution. An ImageJ plugin was used to correct stage position drifting when needed (K. Li, "The image stabilizer plugin for ImageJ," www.cs.cmu.edu/~kangli/code/Image_Stabilizer.html, February 2008). Three customized MATLAB graphical user interface (GUI) tools were used in this study: *Vicinity* (Wu *et al.* 2015) and two newly developed tools, *ROI_TOI* and *BudTrack*, described in detail below:

ROI_TOI (Figure 7) is designed for the fast and convenient setting of a dynamically changing elliptical region of interest (ROI) and subsequent quantification of the fluorescence intensity within that region during a user-specified time of interest (TOI). The analysis works for a single gray-scale channel or for two synchronized channels. The quantification includes mean, maximum, median, summed (total) intensity, coefficient of variation (CV), and other analyses of the pixel intensity distribution.

In this study we used the CV of the pixel intensity for maximum-intensity projections of cell images to measure both Whi5 nuclear exit (see below) and polarization of other probes (Bem1, Cdc3, or Sec4). For any given cell, the CV measure tracked closely with a measurement of the total probe signal intensity measured in a circle with radius 1.5 µm at the polarity site (background subtracted) using a previously published tool, *Vicinity* (Wu *et al.*, 2015; Supplemental Figure S1). However, the CV measure is sensitive to overall cell size as well as local probe accumulation (Supplemental Figure S1F): if a small cell and a large cell accumulated the same amount of probe at the polarity site, the CV would report a higher value for the small cell, because the large cell would have a greater number of pixels with uniform intensity outside the polarity site. Thus, the CV measure effectively reports the proportion of the total cellular probe that accumulates at the polarity site rather than the absolute amount of probe.

To allow determination of the timing of 50% Whi5 nuclear exit (i.e., Start), *ROI_TOI* is designed to identify a "peak duration" defined as one of the following: 1) the time interval for which the

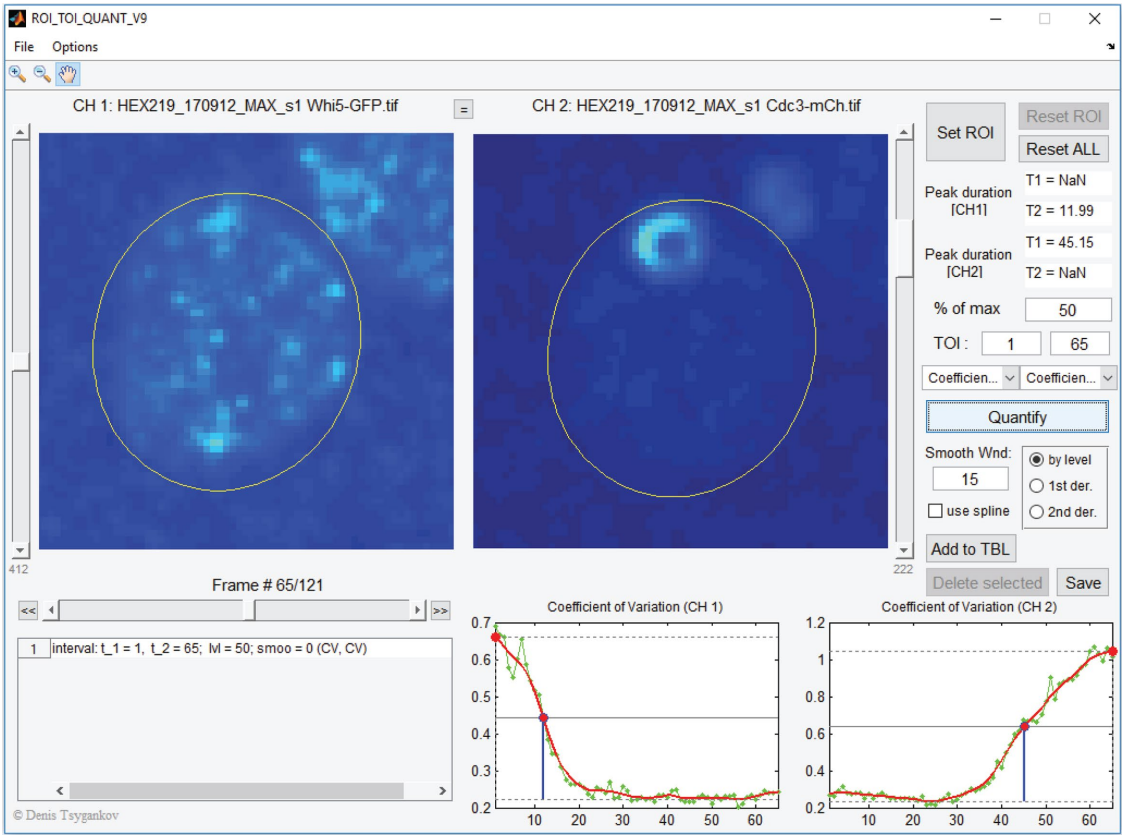

FIGURE 7: Screenshot illustrating the customized image analysis tool *ROI_TOI*. The upper left shows two maximum projection *z*-stacks from two fluorescent channels of a time-lapse imaging (Whi5-GFP and Cdc3-mCherry in this case). The upper right column allows the user to specify a cell by creating an elliptical region of interest (ROI), the type of analysis (coefficient of variation level in this case), the percent of max at which to determine the peak duration (50% in this case), the time of interest (TOI), and the smooth parameter. After the user clicks the "Quantify" button, the upper right column indicates "T2," which is the interpolated time point (11.99 in this case) at which Whi5-GFP is at 50% with a negative slope. The bottom right shows the results for the two channels, and the bottom left is where the list of results is temporarily stored before being saved.

measure of interest (here Whi5 CV) is above a user-defined percentage of the difference between the maximum and minimum value of the signal throughout the TOI, 2) the time interval between the highest and the lowest values of the first derivative of the measure, or 3) the time interval between the two nearest peaks of the second derivative of the measure. The method in 1 was used to determine the timing of Start based on when the CV for Whi5-GFP dropped to 50% of its peak value (Figure 1, A–C).

The two major advantages of this tool are as follows. 1) The elliptical region of interest can be positioned interactively with an arbitrary location, size, and orientation using three mouse-draggable points. 2) By setting the ROIs at selected time frames, the dynamic ROI is automatically created by linear interpolation. The selections can be added at any time frame and removed from any previously set time frame.

Each ROI setting and quantification can be added to the table as a list for subsequent saving of the collected results as a text file. Additional features of the GUI include a zoom-in/-out option, image contrast adjustment, image colormap selection, and the Gaussian smoothing of a measure of interest with a user-defined size of the smoothing window.

BudTrack (Figure 8) is designed for close inspection of the yeast budding process and for accurate detection of the time of bud emergence using fluorescence intensities (such as the plasma membrane probe Psr1(1-28aa)-mCherry used for this study). The GUI provides 3D visualization of a gray-scale *z*-stack of fluorescence data and two modes of analysis: 1) kymograph of the fluorescent signal along the axis of the bud growth and 2) automated fit of the cell-bud geometry with two ellipsoids. The *z*-stack data must be imported as a single tiff file. The user specifies the number of *z*-slices and the resolution ratio of the *z* step to the pixel size in the (*x*,*y*)-plane for proper scaling in the 3D view. The GUI automatically determines a background threshold using the Otsu algorithm, but the resulting value can be changed as needed. The GUI displays the isosurface based on the binary 3D mask that is generated with the specified threshold value.

In the "manual alignment" mode, the user is asked to align the axis of bud growth manually to a horizontal line by adjusting the yaw and pitch angles of rotation. The resulting kymograph is the fluorescent signal in the originally imported file along the central axis of the bud growth (*y*-axis of the kymograph) at each time (*x*-axis of the kymograph).

In the "automated Fitting" mode, the GUI runs an optimization algorithm that minimizes the difference between the isosurface from the segmented data and the surface formed by two ellipsoids. Effectively, the algorithm fits two ellipsoids to the cell-bud shape by adjusting the location and orientation of the ellipsoids. The fitting is sensitive to the quality of the data. Thus, if the data-based isosurface

A

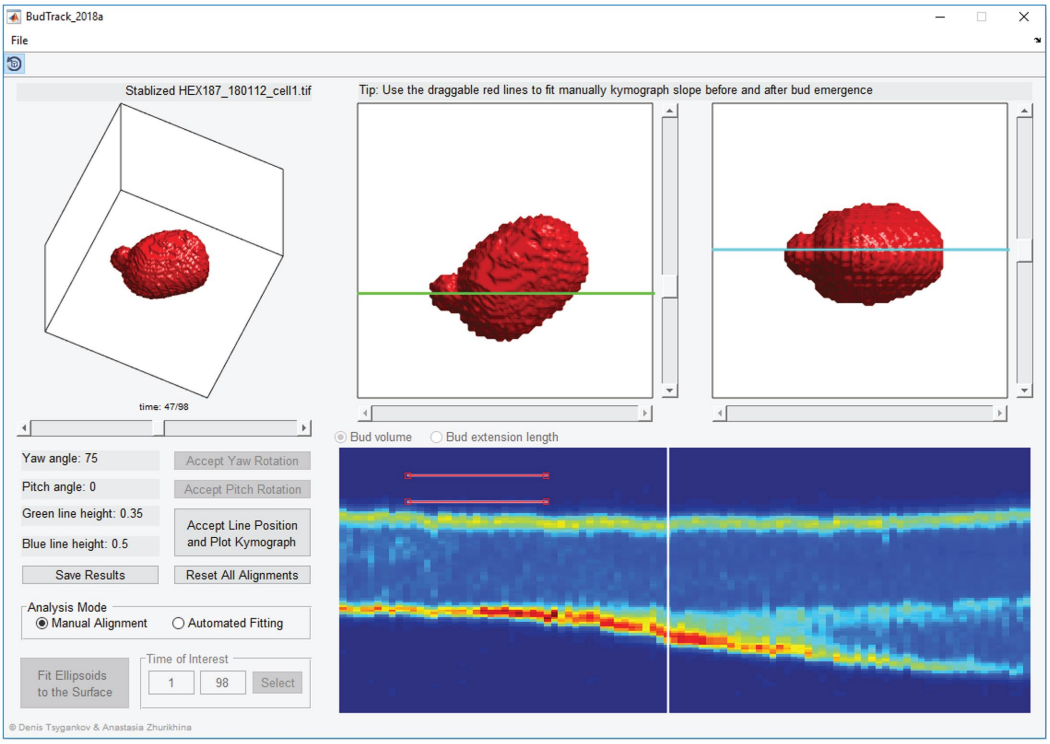

B

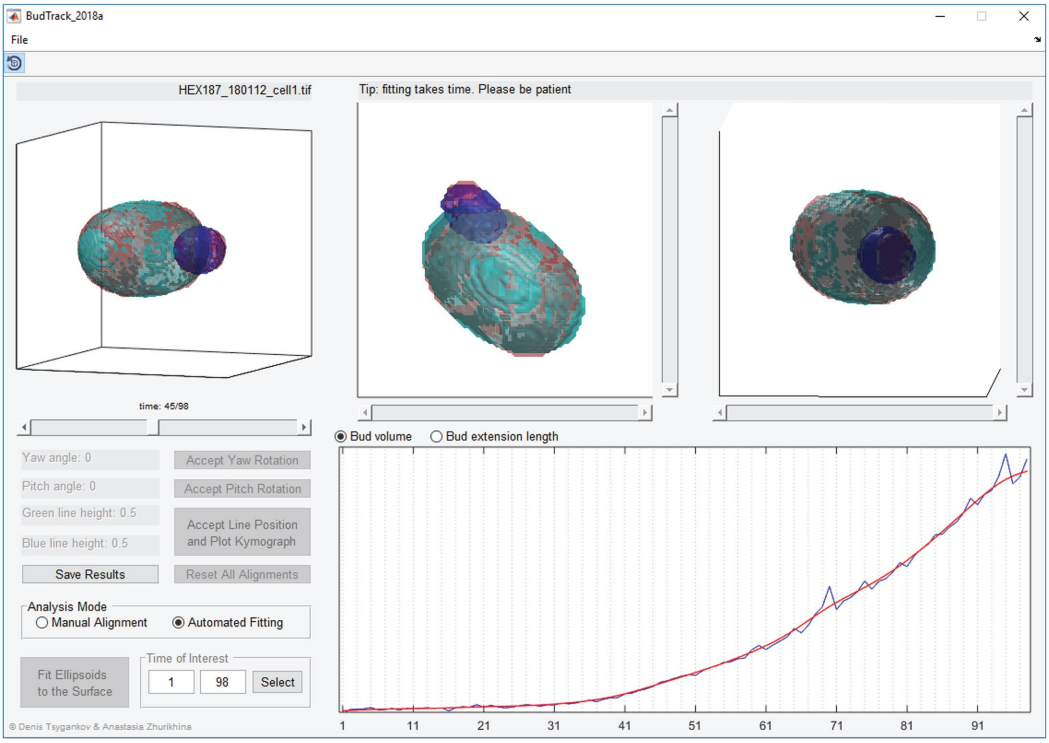

FIGURE 8: Screenshot illustrating the customized image analysis tool *BudTrack*. (A) Manual alignment mode: the upper left is the 3D cell surface rendering constructed from a *z*-stack of a cell expressing the fluorescent plasma membrane probe, Psr1(1-28aa)-mCherry. The upper middle and right channels are the same cell viewed from two different angles to allow alignment of the mother-bud axis. The bottom left shows the control panel and provides information on the alignment settings. The bottom right illustrates the kymograph rendering for the aligned cell (white line corresponds to the time point for cell shown in the upper panels). (B) Automated fitting mode: the layout of the program is the same as in A, except in this case automated fitting was selected. The original 3D cell surface rendering is represented in transparent red. The ellipses fitted to the mother cell and bud are represented in the top panels in transparent cyan and dark blue, respectively. The change in fitted bud volume over time is shown in the bottom right panel.

does not look like an intersection of two ellipsoids to begin with, the kymograph mode should be favored over this type of analysis. Otherwise, this method provides a measure of the bud volume and its extension length (the distance from the base to the tip of the bud) in an automatic and unbiased manner. The volume is smoothed using standard Gaussian filtering and displayed together with the unsmoothed measurement.

ACKNOWLEDGMENTS

We thank Bruce Goode for the gift of the mCherry-Sec4 plasmid and Lisa Cameron and Yasheng Gao at the Duke University Light Microscopy Core Facility for their continuous assistance in image acquisition and trouble-shooting. Both former and current Lew lab members provided immense support and stimulating discussion throughout the project. This work was supported by National Institutes of Health/National Institute of General Medical Sciences Grants GM62300 and GM122488 to D.J.L. and by U.S. Army Research Office (ARO) Grant W911NF-17-1-0395 to D.T.

REFERENCES

Adams AE, Johnson DI, Longnecker RM, Sloat BF, Pringle JR (1990). CDC42 and CDC43, two additional genes involved in budding and the establishment of cell polarity in the yeast *Saccharomyces cerevisiae*. J Cell Biol 111, 131–142.

Adams AE, Pringle JR (1984). Relationship of actin and tubulin distribution to bud growth in wild-type and morphogenetic-mutant *Saccharomyces cerevisiae*. J Cell Biol 98, 934–945.

Ayscough KR, Stryker J, Pokala N, Sanders M, Crews P, Drubin DG (1997). High rates of actin filament turnover in budding yeast and roles for actin in establishment and maintenance of cell polarity revealed using the actin inhibitor latrunculin-A. J Cell Biol 137, 399–416.

Baudin A, Ozier-Kalogeropoulos O, Denouel A, Lacroute F, Cullin C (1993). A simple and efficient method for direct gene deletion in Saccharomyces cerevisiae. Nucleic Acids Res 21, 3329–3330.

Bender A, Pringle JR (1989). Multicopy suppression of the cdc24 budding defect in yeast by CDC42 and three newly identified genes including the ras-related gene RSR1. Proc Natl Acad Sci USA 86, 9976–9980.

Berg JM, Tymoczko JL, Gatto GJ, Stryer L (2015). Biochemistry, New York: Freeman.

Bi E, Pringle JR (1996). ZDS1 and ZDS2, genes whose products may regulate Cdc42p in Saccharomyces cerevisiae. Mol Cell Biol 16, 5264–5275.

Bryan AK, Goranov A, Amon A, Manalis SR (2010). Measurement of mass, density, and volume during the cell cycle of yeast. Proc Natl Acad Sci USA 107, 999–1004.

Caviston JP, Longtine M, Pringle JR, Bi E (2003). The role of Cdc42p GTPase-activating proteins in assembly of the septin ring in yeast. Mol Biol Cell 14, 4051–4066.

Chen H, Howell AS, Robeson A, Lew DJ (2011). Dynamics of septin ring and collar formation in *Saccharomyces cerevisiae*. Biol Chem 392, 689–697.

Chen H, Kuo CC, Kang H, Howell AS, Zyla TR, Jin M, Lew DJ (2012). Cdc42p regulation of the yeast formin Bni1p mediated by the effector Gic2p. Mol Biol Cell 23, 3814–3826.

Chesarone MA, Goode BL (2009). Actin nucleation and elongation factors: mechanisms and interplay. Curr Opin Cell Biol 21, 28–37.

Chiou JG, Balasubramanian MK, Lew DJ (2017). Cell polarity in yeast. Annu Rev Cell Dev Biol 33, 77–101.

Costanzo M, Nishikawa JL, Tang X, Millman JS, Schub O, Breitkreuz K, Dewar D, Rupes I, Andrews B, Tyers M (2004). CDK activity antagonizes Whi5, an inhibitor of G1/S transcription in yeast. Cell 117, 899–913.

Cvrckova F, De Virgilio C, Manser E, Pringle JR, Nasmyth K (1995). Ste20-like protein kinases are required for normal localization of cell growth and for cytokinesis in budding yeast. Genes Dev 9, 1817–1830.

de Bruin RA, McDonald WH, Kalashnikova TI, Yates J 3rd, Wittenberg C (2004). Cln3 activates G1-specific transcription via phosphorylation of the SBF bound repressor Whi5. Cell 117, 887–898.

DeMarini DJ, Adams AE, Fares H, De Virgilio C, Valle G, Chuang JS, Pringle JR (1997). A septin-based hierarchy of proteins required for localized deposition of chitin in the *Saccharomyces cerevisiae* cell wall. J Cell Biol 139, 75–93.

Denis V, Cyert MS (2005). Molecular analysis reveals localization of *Saccharomyces cerevisiae* protein kinase C to sites of polarized growth and Pkc1p targeting to the nucleus and mitotic spindle. Eukaryot Cell 4, 36–45.

Di Talia S, Skotheim JM, Bean JM, Siggia ED, Cross FR (2007). The effects of molecular noise and size control on variability in the budding yeast cell cycle. Nature 448, 947–951.

Doncic A, Falleur-Fettig M, Skotheim JM (2011). Distinct interactions select and maintain a specific cell fate. Mol Cell 43, 528–539.

Donovan KW, Bretscher A (2015). Tracking individual secretory vesicles during exocytosis reveals an ordered and regulated process. J Cell Biol 210, 181–189.

Drgonova J, Drgon T, Tanaka K, Kollar R, Chen GC, Ford RA, Chan CS, Takai Y, Cabib E (1996). Rho1p, a yeast protein at the interface between cell polarization and morphogenesis. Science 272, 277–279.

Egelhofer TA, Villen J, McCusker D, Gygi SP, Kellogg DR (2008). The septins function in G1 pathways that influence the pattern of cell growth in budding yeast. PLoS One 3, e2022.

Gao XD, Sperber LM, Kane SA, Tong Z, Tong AH, Boone C, Bi E (2007). Sequential and distinct roles of the cadherin domain-containing protein Axl2p in cell polarization in yeast cell cycle. Mol Biol Cell 18, 2542–2560.

Gladfelter AS, Kozubowski L, Zyla TR, Lew DJ (2005). Interplay between septin organization, cell cycle and cell shape in yeast. J Cell Sci 118, 1617–1628.

Gonzalez-Novo A, Correa-Bordes J, Labrador L, Sanchez M, Vazquez de Aldana CR, Jimenez J (2008). Sep7 is essential to modify septin ring dynamics and inhibit cell separation during *Candida albicans* hyphal growth. Mol Biol Cell 19, 1509–1518.

Goranov AI, Cook M, Ricicova M, Ben-Ari G, Gonzalez C, Hansen C, Tyers M, Amon A (2009). The rate of cell growth is governed by cell cycle stage. Genes Dev 23, 1408–1422.

Gray JV, Ogas JP, Kamada Y, Stone M, Levin DE, Herskowitz I (1997). A role for the Pkc1 MAP kinase pathway of *Saccharomyces cerevisiae* in bud emergence and identification of a putative upstream regulator. EMBO J 16, 4924–4937.

Gulli MP, Jaquenoud M, Shimada Y, Niederhauser G, Wiget P, Peter M (2000). Phosphorylation of the Cdc42 exchange factor Cdc24 by the PAK-like kinase Cla4 may regulate polarized growth in yeast. Mol Cell 6, 1155–1167.

Harold FM (1990). To shape a cell: an inquiry into the causes of morphogenesis of microorganisms. Microbiol Rev 54, 381–431.

Harold FM (2002). Force and compliance: rethinking morphogenesis in walled cells. Fungal Genet Biol 37, 271–282.

Howell AS, Jin M, Wu CF, Zyla TR, Elston TC, Lew DJ (2012). Negative feedback enhances robustness in the yeast polarity establishment circuit. Cell 149, 322–333.

Howell AS, Lew DJ (2012). Morphogenesis and the cell cycle. Genetics 190, 51–77.

Iwase M, Luo J, Nagaraj S, Longtine M, Kim HB, Haarer BK, Caruso C, Tong Z, Pringle JR, Bi E (2006). Role of a Cdc42p effector pathway in recruitment of the yeast septins to the presumptive bud site. Mol Biol Cell 17, 1110–1125.

Kadota J, Yamamoto T, Yoshiuchi S, Bi E, Tanaka K (2004). Septin ring assembly requires concerted action of polarisome components, a PAK kinase Cla4p, and the actin cytoskeleton in Saccharomyces cerevisiae. Mol Biol Cell 15, 5329–5345.

Ketela T, Green R, Bussey H (1999). *Saccharomyces cerevisiae* mid2p is a potential cell wall stress sensor and upstream activator of the PKC1-MPK1 cell integrity pathway. J Bacteriol 181, 3330–3340.

Kohli M, Galati V, Boudier K, Roberson RW, Philippsen P (2008). Growth-speed-correlated localization of exocyst and polarisome components in growth zones of *Ashbya gossypii* hyphal tips. J Cell Sci 121, 3878–3889.

Kono K, Nogami S, Abe M, Nishizawa M, Morishita S, Pellman D, Ohya Y (2008). G1/S cyclin-dependent kinase regulates small GTPase Rho1p through phosphorylation of RhoGEF Tus1p in *Saccharomyces cerevisiae*. Mol Biol Cell 19, 1763–1771.

Kozubowski L, Larson JR, Tatchell K (2005). Role of the septin ring in the asymmetric localization of proteins at the mother-bud neck in *Saccharomyces cerevisiae*. Mol Biol Cell 16, 3455–3466.

Kozubowski L, Saito K, Johnson JM, Howell AS, Zyla TR, Lew DJ (2008). Symmetry-breaking polarization driven by a Cdc42p GEF-PAK complex. Curr Biol 18, 1719–1726.

Krause SA, Cundell MJ, Poon PP, McGhie J, Johnston GC, Price C, Gray JV (2012). Functional specialisation of yeast Rho1 GTP exchange factors. J Cell Sci 125, 2721–2731.

Kuo CC, Savage NS, Chen H, Wu CF, Zyla TR, Lew DJ (2014). Inhibitory GEF phosphorylation provides negative feedback in the yeast polarity circuit. Curr Biol 24, 753–759.

Lee ME, Lo WC, Miller KE, Chou CS, Park HO (2015). Regulation of Cdc42 polarization by the Rsr1 GTPase and Rga1, a Cdc42 GTPase-activating protein, in budding yeast. J Cell Sci 128, 2106–2117.
Lee PR, Song S, Ro HS, Park CJ, Lippincott J, Li R, Pringle JR, De Virgilio C, Longtine MS, Lee KS (2002). Bni5p, a septin-interacting protein, is required for normal septin function and cytokinesis in *Saccharomyces cerevisiae*. Mol Cell Biol 22, 6906–6920.
Lesage G, Bussey H (2006). Cell wall assembly in *Saccharomyces cerevisiae*. Microbiol Mol Biol Rev 70, 317–343.
Levin DE (2005). Cell wall integrity signaling in *Saccharomyces cerevisiae*. Microbiol Mol Biol Rev 69, 262–291.
Lew DJ, Reed SI (1995). A cell cycle checkpoint monitors cell morphogenesis in budding yeast. J Cell Biol 129, 739–749.
Li CR, Au Yong JY, Wang YM, Wang Y (2012). CDK regulates septin organization through cell-cycle-dependent phosphorylation of the Nim1-related kinase Gin4. J Cell Sci 125, 2533–2543.
Linnemans WA, Boer P, Elbers PF (1977). Localization of acid phosphatase in *Saccharomyces cerevisiae*: a clue to cell wall formation. J Bacteriol 131, 638–644.
Mazur P, Morin N, Baginsky W, el-Sherbeini M, Clemas JA, Nielsen JB, Foor F (1995). Differential expression and function of two homologous subunits of yeast 1,3-beta-D-glucan synthase. Mol Cell Biol 15, 5671–5681.
Merlini L, Bolognesi A, Juanes MA, Vandermoere F, Courtellemont T, Pascolutti R, Seveno M, Barral Y, Piatti S (2015). Rho1- and Pkc1-dependent phosphorylation of the F-BAR protein Syp1 contributes to septin ring assembly. Mol Biol Cell 26, 3245–3262.
Morgan DO (2007). The Cell Cycle: Principles of Control, London: New Science Press.
Mulholland J, Preuss D, Moon A, Wong A, Drubin D, Botstein D (1994). Ultrastructure of the yeast actin cytoskeleton and its association with the plasma membrane. J Cell Biol 125, 381–391.
Oh Y, Bi E (2011). Septin structure and function in yeast and beyond. Trends Cell Biol 21, 141–148.
Okada S, Leda M, Hanna J, Savage NS, Bi E, Goryachev AB (2013). Daughter cell identity emerges from the interplay of Cdc42, septins, and exocytosis. Dev Cell 26, 148–161.
Orlean P (2012). Architecture and biosynthesis of the *Saccharomyces cerevisiae* cell wall. Genetics 192, 775–818.
Pringle JR, Bi E, Harkins HA, Zahner JE, De Virgilio C, Chant J, Corrado K, Fares H (1995). Establishment of cell polarity in yeast. Cold Spring Harbor Symp Quant Biol 60, 729–744.
Pruyne D, Gao L, Bi E, Bretscher A (2004a). Stable and dynamic axes of polarity use distinct formin isoforms in budding yeast. Mol Biol Cell 15, 4971–4989.
Pruyne D, Legesse-Miller A, Gao L, Dong Y, Bretscher A (2004b). Mechanisms of polarized growth and organelle segregation in yeast. Annu Rev Cell Dev Biol 20, 559–591.
Qadota H, Python CP, Inoue SB, Arisawa M, Anraku Y, Zheng Y, Watanabe T, Levin DE, Ohya Y (1996). Identification of yeast Rho1p GTPase as a regulatory subunit of 1,3-beta-glucan synthase. Science 272, 279–281.
Rajavel M, Philip B, Buehrer BM, Errede B, Levin DE (1999). Mid2 is a putative sensor for cell integrity signaling in *Saccharomyces cerevisiae*. Mol Cell Biol 19, 3969–3976.
Ram AF, Brekelmans SS, Oehlen LJ, Klis FM (1995). Identification of two cell cycle regulated genes affecting the beta 1,3-glucan content of cell walls in *Saccharomyces cerevisiae*. FEBS Lett 358, 165–170.
Reed SI (1980). The selection of *S. cerevisiae* mutants defective in the start event of cell division. Genetics 95, 561–577.
Roh DH, Bowers B, Riezman H, Cabib E (2002). Rho1p mutations specific for regulation of beta(1→3)glucan synthesis and the order of assembly of the yeast cell wall. Mol Microbiol 44, 1167–1183.
Schmidt M, Varma A, Drgon T, Bowers B, Cabib E (2003). Septins, under Cla4p regulation, and the chitin ring are required for neck integrity in budding yeast. Mol Biol Cell 14, 2128–2141.
Schott DH, Collins RN, Bretscher A (2002). Secretory vesicle transport velocity in living cells depends on the myosin-V lever arm length. J Cell Biol 156, 35–39.
Sentandreu R, Northcote DH (1969). The formation of buds in yeast. J Gen Microbiol 55, 393–398.
Sinha I, Wang YM, Philp R, Li CR, Yap WH, Wang Y (2007). Cyclin-dependent kinases control septin phosphorylation in *Candida albicans* hyphal development. Dev Cell 13, 421–432.
Sloat BF, Adams A, Pringle JR (1981). Roles of the CDC24 gene product in cellular morphogenesis during the *Saccharomyces cerevisiae* cell cycle. J Cell Biol 89, 395–405.
Smits GJ, Kapteyn JC, van den Ende H, Klis FM (1999). Cell wall dynamics in yeast. Curr Opin Microbiol 2, 348–352.
Tang CS, Reed SI (2002). Phosphorylation of the septin cdc3 in g1 by the cdc28 kinase is essential for efficient septin ring disassembly. Cell Cycle 1, 42–49.
Walworth NC, Brennwald P, Kabcenell AK, Garrett M, Novick P (1992). Hydrolysis of GTP by Sec4 protein plays an important role in vesicular transport and is stimulated by a GTPase-activating protein in *Saccharomyces cerevisiae*. Mol Cell Biol 12, 2017–2028.
Woods B, Lai H, Wu CF, Zyla TR, Savage NS, Lew DJ (2016). Parallel actin-independent recycling pathways polarize Cdc42 in budding yeast. Curr Biol 26, 2114–2126.
Wu CF, Chiou JG, Minakova M, Woods B, Tsygankov D, Zyla TR, Savage NS, Elston TC, Lew DJ (2015). Role of competition between polarity sites in establishing a unique front. eLife 4.
Zheng Y, Cerione R, Bender A (1994). Control of the yeast bud-site assembly GTPase Cdc42. Catalysis of guanine nucleotide exchange by Cdc24 and stimulation of GTPase activity by Bem3. J Biol Chem 269, 2369–2372.